CHAPTER 2

MARANGONI INSTABILITY IN A LIQUID LAYER CONFINED BETWEEN TWO CONCENTRIC SPHERICAL SURFACES

2.1 Introduction.

When a solute evaporates from a liquid at a gas/liquid interface and the liquid's surface tension depends on the solute concentration, spontaneous liquid motion can arise which can develop into a roll-cell pattern in the liquid. This phenomenon is called Marangoni convection. In mass-transfer equipment, Marangoni convection enhances mass transfer because convective flows in the liquid reduce the resistance against mass transfer in the liquid. To study this important effect, the Department of Chemical Engineering of the University of Groningen, The Netherlands, has performed several experiments with ventilated air bubbles in an acetone in water solution. Acetone evaporates from the liquid to the gas phase and, since the surface tension is a decreasing function of the acetone concentration, Marangoni instability can be expected to occur and was actually recorded. These experiments were performed under micro-gravity conditions in order to eliminate buoyancy effects. For further details we refer to Lichtenbelt et al. (1986) and Dijkstra and Lichtenbelt (1988).

Two types of Marangoni convection can be distinguished: macro- and microscale convection. The former is due to macroscopic surface-tension gradients being initially present in the system, the latter develops because the system is hydrodynamically unstable, that is, small perturbations of some given initial state of the system will grow in time. In this paper we study the onset of microscale Marangoni convection in a liquid layer confined between two concentric spheres. The inner sphere is a gas/liquid interface at which a single solute evaporates, the outer sphere is taken to be rigid, and further we assume zero-gravity conditions. We are especially interested in the influence of the curvature of the interface.

For systems with a cylindrical gas/liquid interface this influence was studied in Chapter 1 of this thesis. A first attempt for a spherical interface was made by Pirotte and Lebon (1988). However,

the results presented in Pirotte and Lebon (1988) were erroneous, and they were corrected by Hoefsloot and Hoogstraten (1989). In Chapter 1 and in Pirotte and Lebon (1988) only the stability of a steady-state concentration (or temperature) profile was considered. In this chapter we shall consider the stability of the time-dependent concentration profile in a motionless liquid by "freezing" this profile at a certain time.

In Section 2.2 we give the mathematical formulation of the problem and perform a linear stability analysis using a standard normal-mode approach. Numerical results are presented in Section 2.3 and discussed in Section 2.4. Finally, some conclusions are drawn in Section 2.5.

2.2 Mathematical formulation and stability analysis.

Under zero-gravity conditions a layer of liquid containing a single solute is confined between two concentric spheres. The inner spherical surface, located at r=a, is a gas/liquid interface at which the solute evaporates from the liquid to the gas. This interface is assumed to remain fixed at r=a, even in the presence of liquid motion. The outer surface r=a+H is a solid boundary. The liquid is taken to be incompressible and Newtonian and its physical properties will be assumed to be independent of the solute concentration $\tilde{c}$, except for the surface tension γ which will be taken as a decreasing linear function of $\tilde{c}$ in the range of concentration values under consideration.

Initially, at time t=0, the liquid layer has a uniform concentration c_0. Two different cases will be distinguished in this paper: in case 1 we assume the solid outher boundary to be an impervious surface and in case 2 the concentration is taken to be always equal to c_0 at this boundary. In the absence of liquid motion a spherically-symmetric time-dependent concentration profile $c_i(r,t)$ will develop by diffusion only. The index i is equal to 1 or 2 and it refers to the cases 1 and 2, respectively. In case 1 we have $c_1 \to 0$ for $t \to \infty$, because all solute will have evaporated then. When $t \to \infty$ in case 2, the concentration profile $c_2(r,t)$ will tend to a non-zero steady profile $c_\infty(r)$.

We want to investigate the onset of surface-tension driven convective flows in the layer (Marangoni instability). To that end we

apply a linear stability analysis to a concentration profile "frozen" at some time instant $t=t_0$: $c_f(r)=c_i(r,t_0)$, i=1 or 2. Since the time rate of change of infinitesimally small perturbations is generally much larger than that for the underlying unperturbed diffusion process, this approach is justified. At t=0 the liquid layer is unconditionally stable and the above approach allows one to determine the time at which instability will occur first. Furthermore we shall study the stability of the steady concentration profile $c_\infty(r)$ that will develop by diffusion only for $t\to\infty$ in case 2.

To begin with the stability analysis the governing equations of the diffusion-convection problem are linearized about an unperturbed state characterized by zero flow velocity and pressure gradient and by a basic concentration profile $c_b(r)$ representing either $c_f(r)$ or $c_\infty(r)$:

$$\nabla\cdot\vec{v} = 0 \ , \qquad \text{(liquid mass balance)} \qquad (2.1)$$

$$\rho\frac{\partial\vec{v}}{\partial t} = -\nabla p + \mu\nabla^2\vec{v} \ , \qquad \text{(momentum balance)} \qquad (2.2)$$

$$\frac{\partial c}{\partial t} + u\frac{dc_b}{dr} = \mathbb{D}\nabla^2 c. \qquad \text{(solute mass balance)} \qquad (2.3)$$

Here $\vec{v}$ denotes the velocity (with radial component u), p and c are the perturbation pressure and solute concentration and ρ, μ and $\mathbb{D}$ are, respectively, the liquid density, dynamic viscosity and diffusion coefficient.

Next the problem is made dimensionless by scaling the radial coordinate r by the fixed layer thickness H, times t and t_0 by $H^2/\mathbb{D}$, velocities $\vec{v}$ and u by $\mathbb{D}/H$, pressure p by $\rho\mathbb{D}^2/H^2$, and concentrations c, c_b, c_f, c_i and c_∞ by c_0. Applying twice the curl operator to the momentum equation and subsequently taking the inner product with the radius vector (Chandraseker, 1961; Pirotte and Lebon, 1988) one obtains two dimensionless equations for the perturbation fields in spherical coordinates,

$$\nabla^2(Sc^{-1}\frac{\partial}{\partial t} - \nabla^2)(ru) = 0, \qquad (2.4)$$

$$(\frac{\partial}{\partial t} - \nabla^2)c = -u\frac{dc}{dr}_b, \qquad (2.5)$$

where we have used the same notation for the nondimensional variables as for the corresponding dimensional ones and where $Sc=\mu/(\rho\mathbb{D})$ denotes

the Schmidt number. The Laplacian ∇^2 in spherical coordinates (r,θ,φ) reads

$$\nabla^2 = \frac{1}{r^2}\frac{\partial}{\partial r}\left(r^2\frac{\partial}{\partial r}\right) - \frac{1}{r^2}\mathfrak{L}^2, \quad \mathfrak{L}^2 = \frac{-1}{\sin\theta}\frac{\partial}{\partial\theta}\left(\sin\theta\frac{\partial}{\partial\theta}\right) - \frac{1}{\sin^2\theta}\frac{\partial^2}{\partial\varphi^2}. \tag{2.6}$$

At the solid boundary r=1+ a/H we have the boundary conditions

$$u = \frac{\partial u}{\partial r} = 0 \qquad \text{(no-slip condition)}, \tag{2.7}$$

$$\frac{\partial c}{\partial r} = 0 \text{ (case 1), or } c = 0 \text{ (case 2)}, \tag{2.8}$$

and at the gas/liquid interface r=a/H the following conditions should be satisfied:

$$u = 0 \qquad \text{(fixed position of the interface)}, \tag{2.9}$$

$$\frac{\partial c}{\partial r} = \mathrm{Bi}\, c \qquad \text{(mass-transfer condition)}, \tag{2.10}$$

$$\frac{\partial^2 (ru)}{\partial r^2} = \frac{1}{r}\,\mathrm{Ma}\,\mathfrak{L}^2 c \qquad \text{(tangential-stress balance)}. \tag{2.11}$$

In condition (2.10) we have introduced the Biot number Bi; a large (small) value of Bi means that the ratio of the resistance against mass transfer in the gas phase to the resistance in the liquid phase is small (large). The Marangoni number Ma appears in boundary condition (2.11) (see Pirotte and Lebon, 1988). It is defined as

$$\mathrm{Ma} = -\frac{(d\gamma/d\tilde{c})\, c_0\, H}{\mu\, \mathbb{D}}, \tag{2.12}$$

and it is a measure for the ratio of surface-tension forces and viscous forces. If a system has a high value of Ma, the system tends to surface tension driven flows sooner then if the system has a low Ma-value.

Applying the standard normal-mode technique, we write the solution of boundary-value problem (2.4)-(2.11) in separated form:

$$ru(r,\theta,\varphi,t) = U(r)\, Y_n^m(\theta,\varphi)\, e^{\beta t}, \tag{2.13}$$

$$c(r,\theta,\varphi,t) = C(r)\, Y_n^m(\theta,\varphi)\, e^{\beta t}, \quad m, n = 1,2,3,\ldots, \tag{2.14}$$

where $Y_n^m(\theta,\varphi)$ are spherical surface harmonics of the first kind Abromowitz and Stegun (1965) satisfying the equation

$\nabla^2 Y_n^m(\theta,\varphi) = n(n+1) Y_n^m(\theta,\varphi)$. The functions U and C denote the amplitude of the velocity and concentration perturbation, respectively, and β is the (complex) stability parameter that determines the growth or decay in time of the mode. As in Chapter 1, we are only interested in determining the conditions for neutral stability. We can characterize neutral stability by putting β equal to zero.

Substitution of (2.13), (2.14) with $\beta=0$ in equations (2.4) and (2.5) leads to two ordinary differential equations for U(r) and C(r),

$$\mathfrak{D}\,\mathfrak{D}\,U = 0\ , \tag{2.15}$$

$$\mathfrak{D}\,C = \frac{U}{r}\frac{dc_b}{dr}, \tag{2.16}$$

where

$$\mathfrak{D} = \frac{d^2}{dr^2} + \frac{2}{r}\frac{d}{dr} - \frac{n(n+1)}{r^2}\ .$$

Notice that the Schmidt number Sc has disappeared from the problem. The pertinent boundary conditions for (2.15) and (2.16) follow from (2.7)-(2.11):

$$\left.\begin{aligned} U &= \frac{dU}{dr} = 0 \qquad (2.17)\\ \frac{dC}{dr} &= 0 \quad \text{(case 1)}\ ,\ \text{or}\ C = 0 \quad \text{(case 2)} \qquad (2.18)\end{aligned}\right\} \text{at } r=1+\frac{a}{H},$$

$$\left.\begin{aligned} U &= 0\\ \frac{dC}{dr} &= Bi\ C\\ \frac{d^2U}{dr^2} &= Ma\ \frac{n(n+1)}{r}\ C\end{aligned}\right\} \text{at } r=\frac{a}{H}\ . \tag{2.19}$$

For given $c_b(r)$, a/H, n and Bi, equations (2.15), (2.16) together with conditions (2.17)-(2.19) constitute an eigenvalue problem for the eigenfunctions U and C and eigenvalue Ma. This eigenvalue problem has been solved numerically by a simple shooting technique. The solution of (2.15) satisfying boundary conditions (2.17) can be written as a linear combination of two linearly independent solutions U_1 and U_2:

$$U = B_1 U_1 + B_2 U_2 \tag{2.20}$$

where U_1 and U_2 satisfy the "initial" conditions

$$(U,U',U'',U''') = (0,0,1,0),\ (0,0,0,1), \tag{2.21}$$

respectively, at the solid boundary. In a similar manner the solution of (2.16) satisfying boundary condition (2.18) can be written in terms of two particular solutions C_1 and C_2 and one homogeneous solution C_3,

$$C = B_1C_1 + B_2C_2 + B_3C_3. \tag{2.22}$$

In case 1 the basic solutions C_1, C_2 and C_3 satisfy the condition $(C,C') = (1,0)$ at the solid boundary, and in case 2 they satisfy $(C,C') = (0,1)$ at the same boundary. The five basic solutions involved have been computed by a fourth-order Runge-Kutta method.

Substitution of (2.20) and (2.22) in the remaining boundary conditions (2.19) at the interface r=a/H leads to a set of three homogeneous linear algebraic equations for the integration constants B_1, B_2 and B_3. A nontrivial solution exists only if the coefficient determinant is equal to zero. This yields an equation for Ma of the form

$$\begin{vmatrix} a_{11} & a_{12} & 0 \\ a_{21} & a_{22} & a_{23} \\ b_1Ma+a_{31} & b_2Ma+a_{32} & b_3Ma+a_{33} \end{vmatrix} = 0,$$

in which the a_{ij}'s and b_i's are independent of Ma. Evaluation of the determinant leads to a linear equation from which Ma follows as a function of n, Bi, a/H and t.

2.3 Results.

In order to solve the eigenvalue problem for Ma numerically as described in the previous section, we first need to determine the basic concentration profile $c_b(r)$. If c_b is equal to c_f, which is the time-dependent, spherically-symmetric profile c_i (i=1 or 2) frozen at some time $t=t_0$, we have to solve for i=1 or 2 the diffusion equation

$$\frac{\partial c_i}{\partial t} = \frac{\partial^2 c_i}{\partial r^2} + \frac{2}{r}\frac{\partial c_i}{\partial r} \tag{2.23}$$

with boundary conditions

$$\frac{\partial c_1}{\partial r} = 0 \text{ or } c_2=1 \text{ at } r= \frac{a}{H} + 1,$$
$$\frac{\partial c_1}{\partial r} = Bi\ c_i \text{ at } r= \frac{a}{H}\ , \tag{2.24}$$

and initial condition

$$c_i=1 \text{ at } t =0. \tag{2.25}$$

Initial/boundary-value problem (2.23)-(2.25) has been solved with a standard Crank-Nicolson finite-difference scheme. Concentration profiles c_i are shown in Figures 2.1a-2.4a (case 1) and in Figures 2.5a-2.8a (case 2) for various values of t_0, curvature parameter a/H and Biot number Bi. In Figures 2.1b-2.4b (case 1) and in Figures 2.5b-2.8b (case 2) we show the corresponding Marangoni numbers Ma, computed from the eigenvalue problem (2.15)-(2.19) as a function of the wave number α=nH/a, which is the number of waves per unit of length along the interface. In Table 2.1 (case 1) and Table 2.2 (case 2) we collected critical Marangoni numbers $Ma_c=\min(Ma_n)$,n=1,2,.. and the corresponding critical wave numbers α_c.

If c_b is equal to c_∞ we have a steady diffusion problem: c_∞ should satisfy the ordinary differential equation

$$\frac{d^2c_\infty}{dr^2} + \frac{2}{r}\frac{dc_\infty}{dr} = 0 \tag{2.26}$$

with boundary conditions

$$c_\infty = 1, \text{ at } r= \frac{a}{H} + 1,$$
$$\frac{dc_\infty}{dr} = Bi\ c_\infty\ , \text{ at } r= \frac{a}{H}\ . \tag{2.27}$$

The solution of (2.26) and (2.27) is given by

$$c_\infty(r) = 1 + \frac{Bi\ (a/H)^2}{1+(Bi+1)a/H}\left(1 - \frac{1+a/H}{r}\right). \tag{2.28}$$

In Table 2.3 we show the critical Marangoni numbers with corresponding critical wave numbers when $c_b=c_\infty$ in case 2.

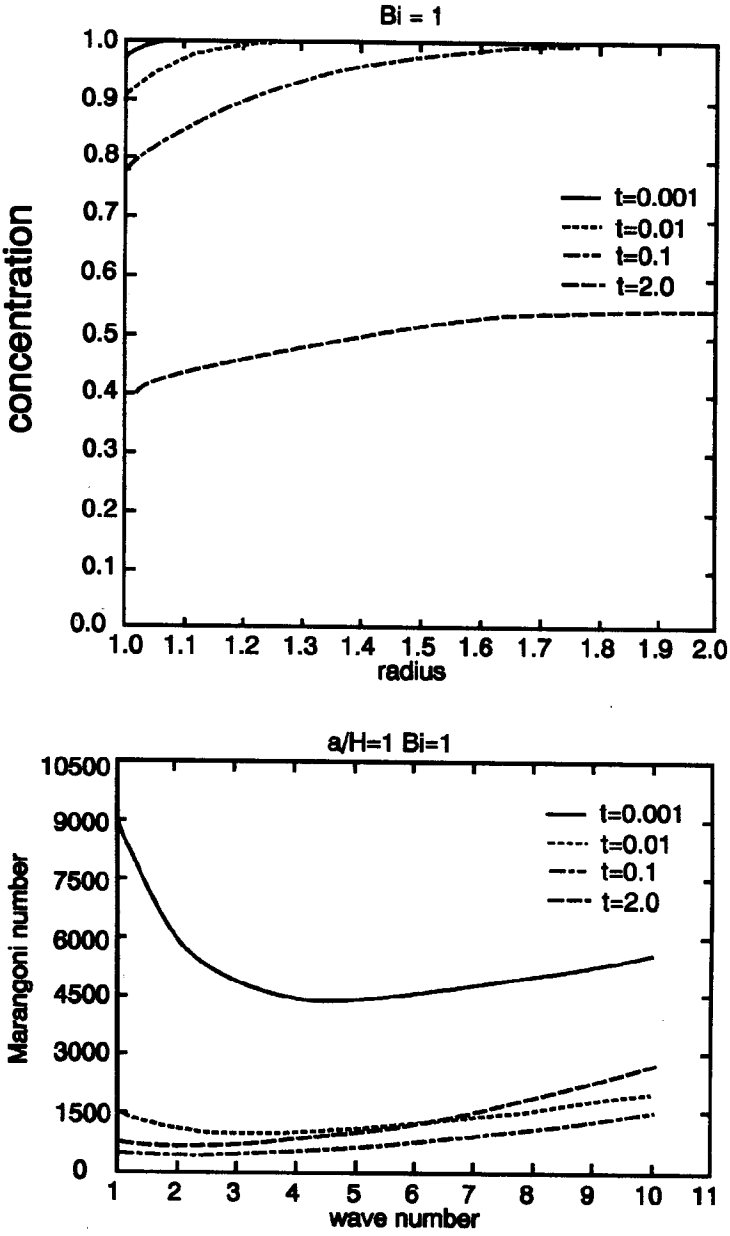

Figure 2.1. *Results for* case 1: a) *concentration profiles* $c_1(r,t)$ *vs. radial coordinate* r *for various values of time* t; b) *neutral-stability curves for Maranogni number* Ma *vs. wavenumber* α (=nH/a) *corresponding to the frozen concentration profiles depicted in Figure* (a). *Parameter values*: Bi=1, a/H=1.

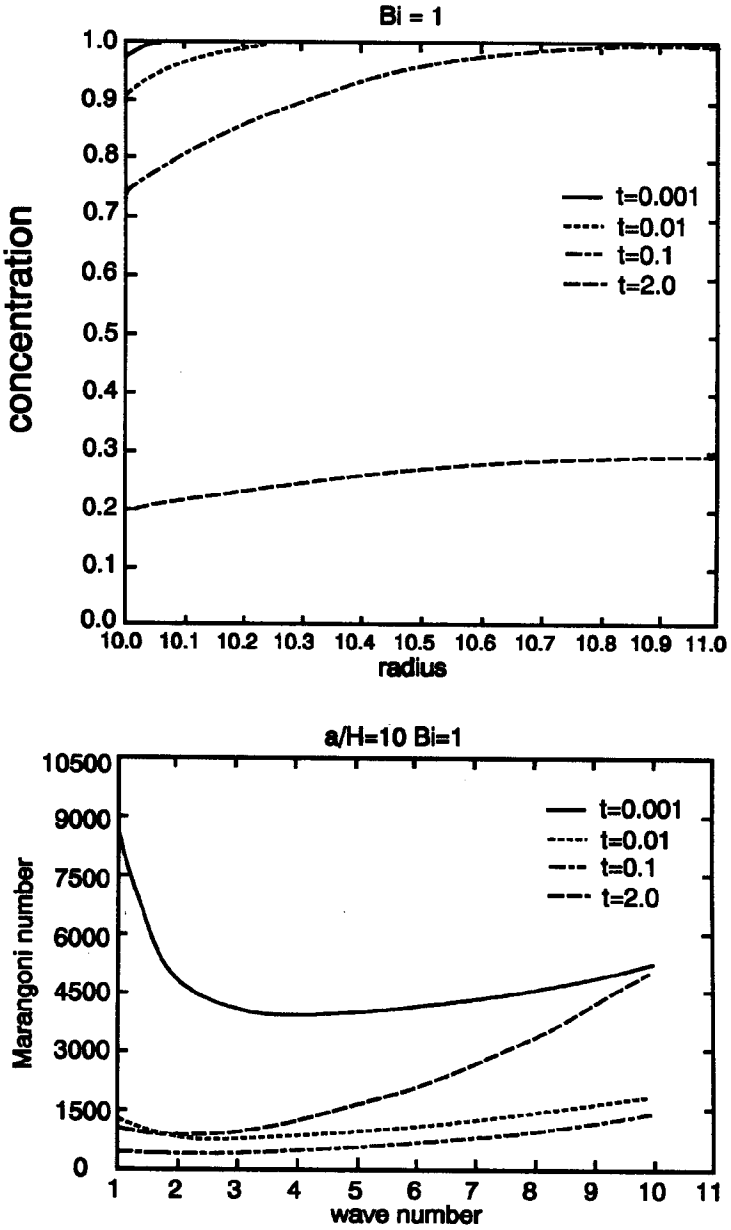

Figure 2.2. *As in* Figure 2.1, *with* Bi=1, a/H=10.

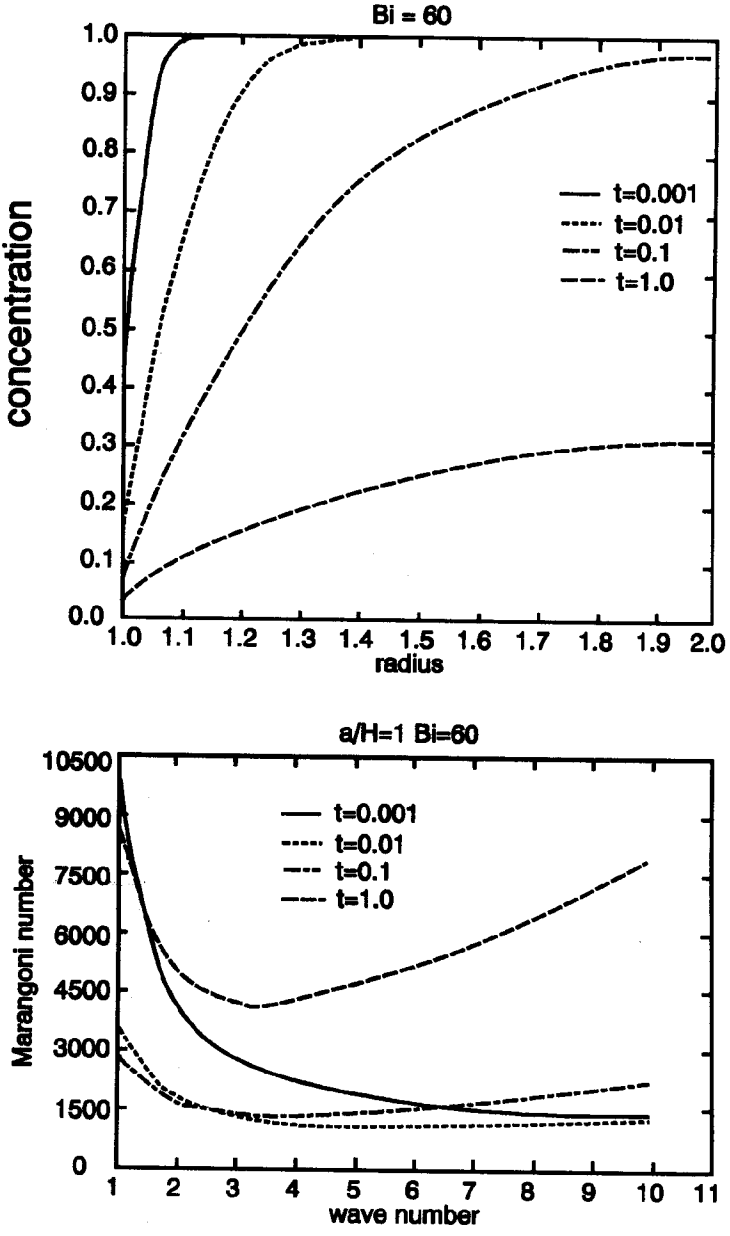

Figure 2.3. *As in* Figure 2.1, *with* Bi=60, a/H=1.

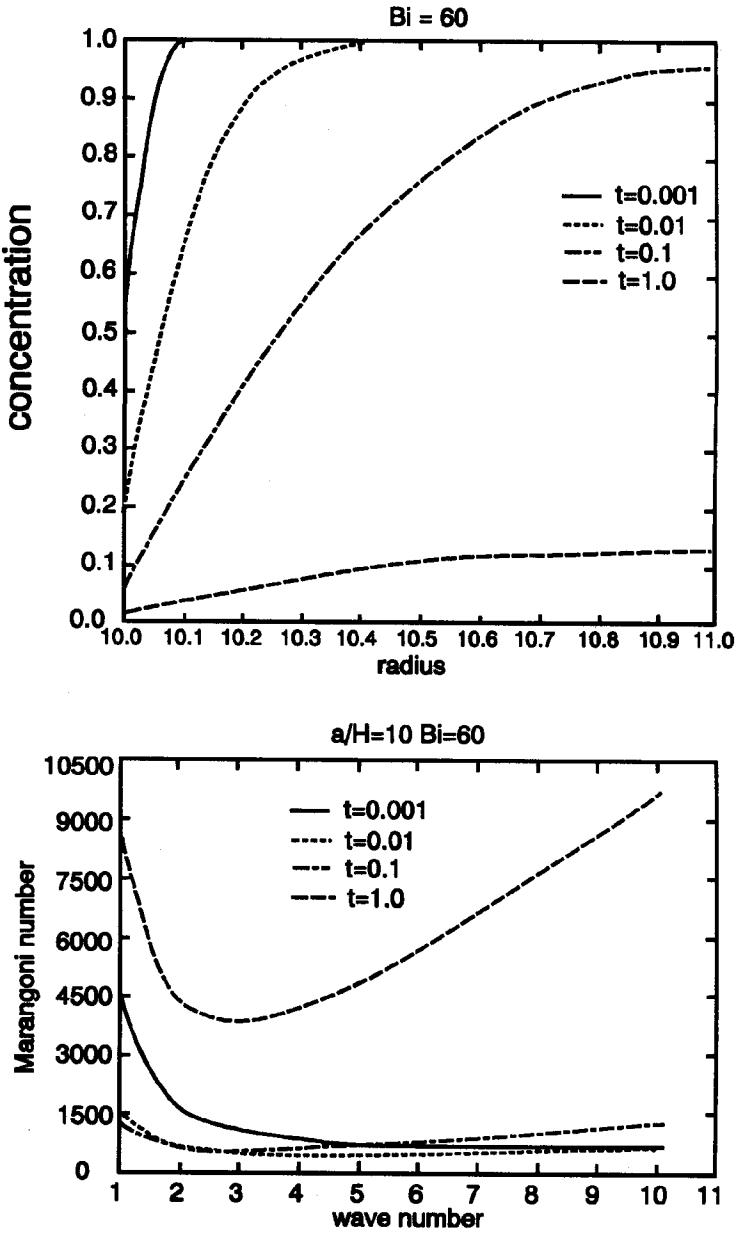

Figure 2.4. *As in* Figure 2.1, *with* Bi=60, a/H=10.

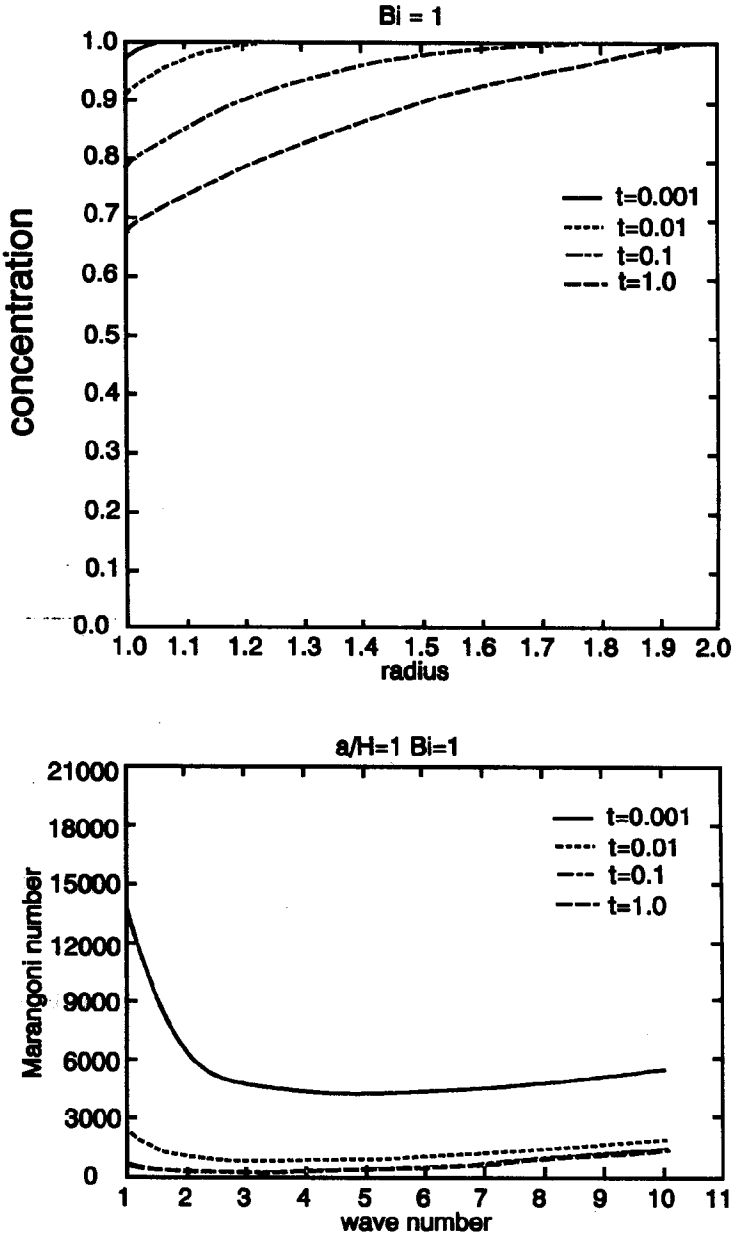

Figure 2.5. *Results for* case 2: a) *concentration profiles* $c_2(r,t)$ *vs. radial coordinate* r *for various values of time* t; b) *neutral stability curves for Marangoni number* Ma *vs. wavenumber* α (=nH/a) *corresponding to the frozen concentration profiles depicted in Figure* (a). *Parameter values*: Bi=1, a/H=1.

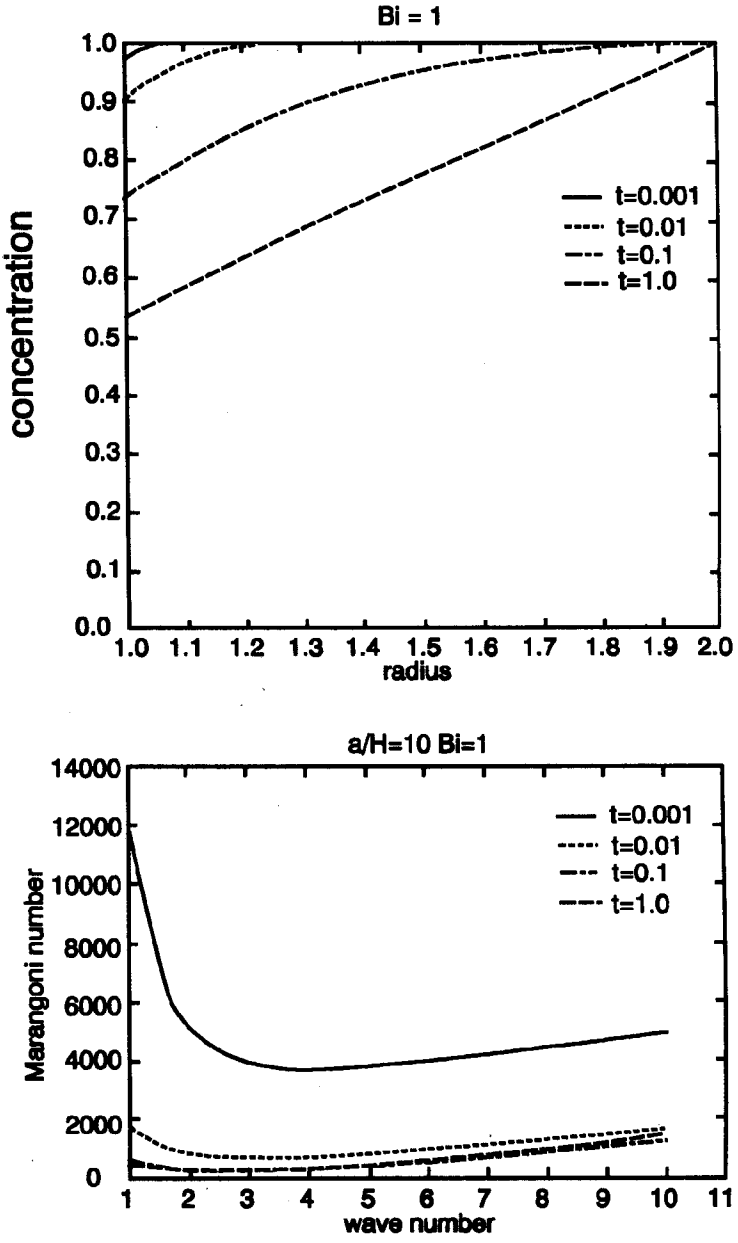

Figure 2.6. *As in* Figure 2.5, *with* Bi=1, a/H=10.

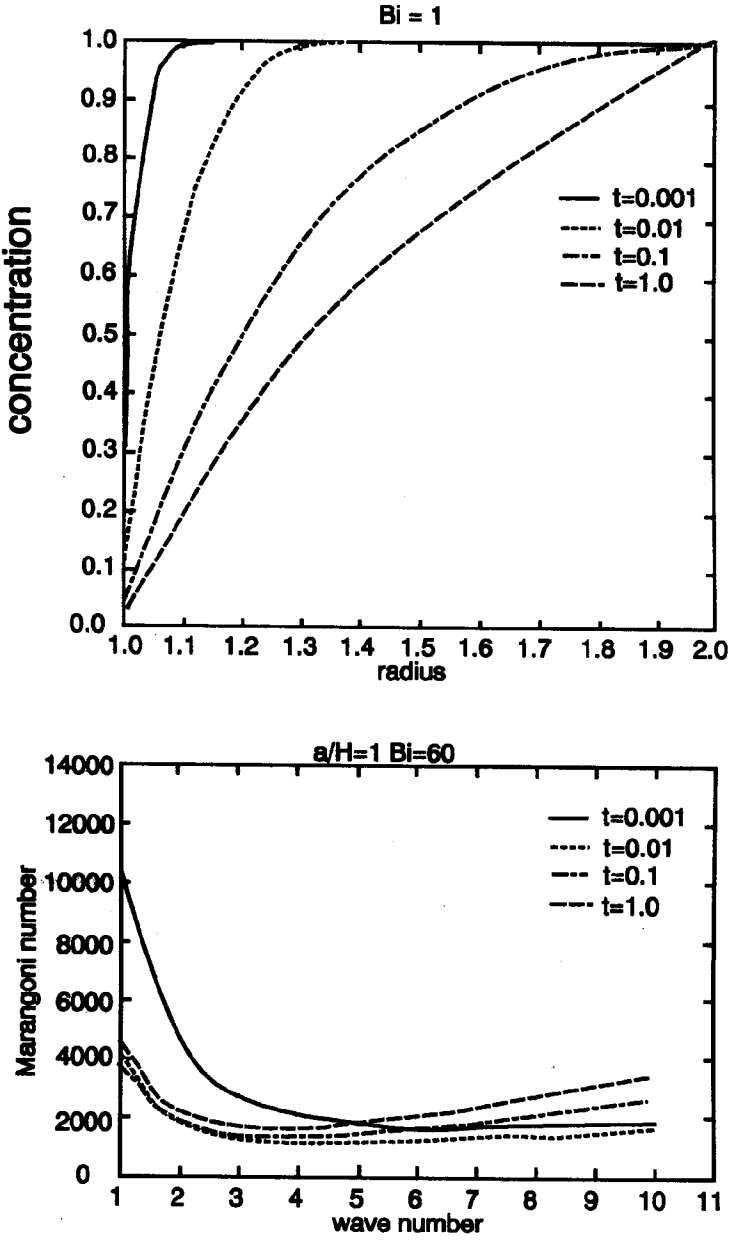

Figure 2.7. *As in* Figure 2.5, *with* Bi=60, a/H=1.

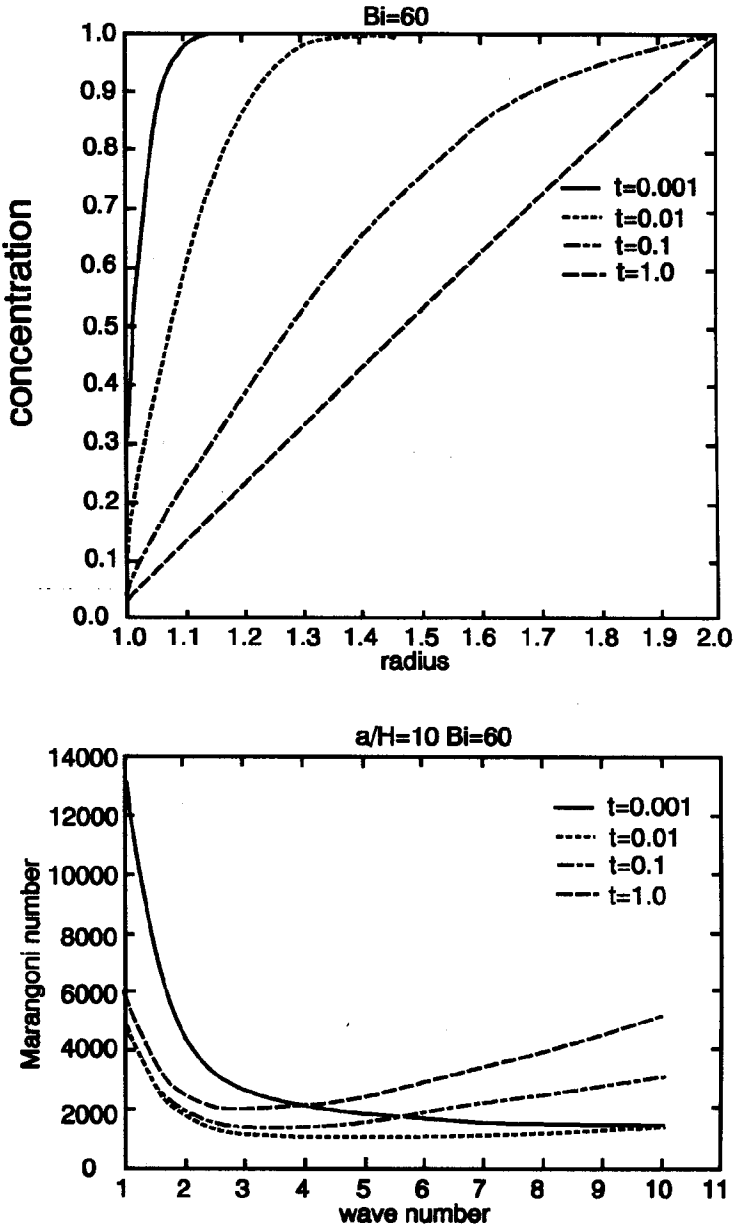

Figure 2.8. *As in* Figure 2.5, *with* Bi=60, a/H=10.

Table 2.1a

	Bi=1				Bi=20			
	a/H=1		a/H=10		a/H=1		a/H=10	
t	Ma_c	α_c	Ma_c	α_c	Ma_c	α_c	Ma_c	α_c
0.001	4425	5	3803	4.0	1071	9	1058	9.0
0.01	955	3	719	2.8	505	5	490	4.3
0.1	394	2	266	2.1	516	4	526	3.0
1.0	445	2	390	1.9	1513	3	3430	2.8
2.0	619	2	764	1.9	4946	3	26965	2.8

Table 2.1b

	Bi=40				Bi=60			
	a/H=1		a/H=10		a/H=1		a/H=10	
t	Ma_c	α_c	Ma_c	α_c	Ma_c	α_c	Ma_c	α_c
0.001	1218	10	1220	10.5	1445	11	1459	11.1
0.01	757	5	761	4.5	1024	5	1046	4.5
0.1	894	4	945	3.1	1240	4	1367	3.1
1.0	2819	4	6843	2.9	4108	4	10265	3.0
2.0	9998	4	59803	2.9	15005	4	93096	3.0

Results for case 1: *critical Marangoni number* Ma_c *and corresponding critical wavenumber* α_c *as a function of time* t *for* Bi=1, 20, 40, 60 *and* a/H=1, 10.

Table 2.2a

	Bi=1				Bi=20			
	a/H=1		a/H=10		a/H=1		a/H=10	
t	Mac	αc	Mac	αc	Mac	αc	Mac	αc
0.001	4436	5	3810	3.9	1071	9	1058	9.0
0.01	981	4	733	3.0	508	5	491	4.3
0.1	443	3	292	2.5	531	4	541	3.2
1.0	383	3	245	2.3	649	4	747	2.9
2.0	383	3	244	2.3	649	4	747	2.9

Table 2.2b

	Bi=40				Bi=60			
	a/H=1		a/H=10		a/H=1		a/H=10	
t	Ma_c	α_c	Ma_c	α_c	Ma_c	α_c	Ma_c	α_c
0.001	1218	10	1220	10.5	1445	11	1459	11.1
0.01	759	5	762	4.5	1028	5	1046	4.6
0.1	901	4	968	3.2	1276	4	1398	3.2
1.0	1115	4	1358	3.0	1585	4	1970	3.0
2.0	1115	4	1358	3.0	1585	4	1970	3.0

Results for case 2: *critical Marangoni number* Ma_c *and corresponding critical wavenumber* α_c *as a function of time* t *for* Bi=1, 20, 40, 60 *and* a/H=1, 10.

Table 2.3

	Bi=1		Bi=20	
a/H	Ma_c	α_c	Ma_c	α_c
0.1	3746	10	921	10
1	383	3	649	4
4	264	2.5	717	3.0
10	244	2.3	747	2.9

Results for steady-state concentration profile in case 2: *critical Marangoni number* Ma_c *and corresponding critical wavenumber* α_c *as a function of the curvature parameter* a/H *for* Bi=1 *and* 20.

2.4 Discussion of results.

First we discuss the results for case 1. At t=0 the system is unconditionally stable ($Ma_c = \infty$) because no concentration gradient is present. Also, for $t \to \infty$, the system is unconditionally stable because then the solute has evaporated completely. Between these two extremes, Ma_c as a function of t first decreases rapidly and after a while increases again. From Table 2.1 we observe that for Bi=1 and Bi=20 the minimum value of Ma_c is lower for a/H=10 than for a/H=1, and also that for small t the rate of decrease of Ma_c is larger for a/H=10 than for a/H=1. For Bi=40 and Bi=60, however, we notice the opposite behaviour, although the differences between a/H=1 and a/H=10 are less pronounced than for Bi=1 and Bi=20. This means that when we consider two systems with different gas-bubble diameter at Biot numbers below, say, 30 and for given system Marangoni number well above the minimum critical value, the system with the largest bubble will show Marangoni instability first. Thus curvature has a stabilizing effect then. For Biot numbers larger than, roughly, Bi=30 the system with the smallest bubble will become unstable first (except for very small values of a/H, as computations have shown). Further we observe that for all values of Bi the critical Marangoni number, after having reached its minimum value, increases more rapidly when a/H=10 than when a/H=1. This can be understood from the concentration profiles at later times, which are much lower for a/H=10 than for a/H=1 (see Figures 2.1a-2.4a). The critical wave number decreases in time. This is caused by the growing in time of the penetration depth of the underlying diffusion process in the liquid, allowing only small perturbation wavelengths for small t, and increasingly larger ones as time progresses.

For small values of t, the results for case 2 strongly resemble those for case 1. Clearly, the diffusion process in the liquid has not had sufficient time to "feel" the difference between the outer-surface boundary condition for the cases 1 and 2. Hence, provided Marangoni instability sets in sufficiently early, we have the same behaviour as in case 1: curvature stabilizes when $Bi \lesssim 30$ and it will have a destabilizing effect when $Bi \gtrsim 30$. As time progresses, the results of cases 1 and 2 become increasingly different: for $t \to \infty$ the results for case 2 tend to those for the steady profile $c_\infty(r)$ for which Ma_c remains finite. It is remarkable that Ma_c decreases

monotonically in time for Bi=1, whereas for Bi=20, 40 ,60 it first decreases and next increases to its asymptotic value for $t \to \infty$.

From Table 2.3 its is seen that for Bi=1 curvature stabilizes the steady state $c_\infty(r)$ and for Bi=20 it has a destabilizing effect (except for very small values of a/H). The switch in behaviour appears to take place around Bi=4. These findings are in agreement with those reported in Chapter 1 for the case of a cylindrical interface.

2.5 Conclusions.

The preceding analysis demonstrates that the onset of micro-scale Marangoni instability in a liquid surrounding a spherical gas bubble and having initially a uniform solute concentration, is influenced by the degree of curvature of the gas/liquid interface. Dependent on the Biot number Bi, increasing curvature can have a stabilizing (or destabilizing) effect in the sense that instability sets in later (or earlier). However, for extremely small gas bubbles, an increase of curvature has always a stabilizing effect. Further, the difference between the boundary conditions at the outer rigid surface for cases 1 and 2 is only noticeable for sufficient large time. In broad terms, the time-dependent stability analysis confirms the more restrictive stability results for the steady state in case 2 and for the steady state in the case of a cylindrical interface (Chapter 1), although the switch in the stabilizing/destabilizing influence of curvature turns out to take place at a significantly larger value of Bi in the time-dependent case.

It has been virtually impossible to observe in the experiments which one of several systems with different gas-bubble diameters showed Marangoni instability first. In all systems instability started almost immediately. The actual system Marangoni numbers were of the order of magnitude of 10^8-10^5, from which it can be concluded on the basis of our time-dependent stability analysis that the instability will start after time interval of in the order of 10^{-2} seconds. Visually, this cannot be distinguished from t=0. In order to be able to observe different times of the onset of instability one should drastically reduce the system Marangoni number. However, it is a very delicate matter to realize this experimentally.